ELSEVIER

Journal of Power Sources 65 (1997) 9–13

JOURNAL OF POWER SOURCES

2

Performance evaluation of $LaNi_{4.7}Al_{0.3}$ and $LaNi_5$ electrodes used as anodes in nickel/metal hydride secondary batteries by analysis of current transients

Su-Il Pyun *, Jeong-Nam Han, Tae-Hyun Yang

Department of Materials Science and Engineering, Korea Advanced Institute of Science and Technology, 373-1 Kusong Dong, Yusong-Gu, Daejon 305-701, South Korea

Received 2 November 1996; accepted 24 November 1996

Abstract

The performance of $LaNi_{4.7}Al_{0.3}$ and $LaNi_5$ porous electrodes used as anodes in nickel/metal hydride secondary batteries has been evaluated by analysis of current decay transients. From the measured three-staged current decay transients for the hydrogen transport through both electrodes in the coexistence of two hydride phases, the discharge capacity and β- to α-phase transition time were determined. The optimum charging condition and velocity of α/β phase boundary movement are discussed with respect to the experimentally obtained discharge capacity and transition time. The potentiostatic current decay transient technique is more conveniently employed to establish the optimum charging condition, as compared with the usual galvanostatic charge–discharge technique.

Keywords: Metal hydrides; Lanthanum–nickel alloy; Electrode reactions

1. Introduction

The nickel/metal hydride (Ni/MH) secondary battery has several advantages such as high energy density per unit volume, long cycle life and reduced environmental problems owing to the absence of such hazardous materials as Pb, Hg and Cd [1–4]. However, there are some problems to be solved for MH electrodes such as passivation of the alloy surface [5], self-discharge [6], hydrogen evolution during high-rate charging [7] and requirement of control of the cut-off of the charging [8].

During the charging and discharging of the Ni/MH cell, MH usually undergoes the phase transformation of hydrogen-poor phase α into hydrogen-rich phase β and vice versa, respectively [9,10]. Recently, it was shown, from current transient analysis, that hydrogen transport through the Pd [11], $LaNi_{4.7}Al_{0.3}$ [12] and $Ni(OH)_2$ [13] electrodes in the coexistence of two hydrogen-poor and -rich phases proceeds by interface-controlled phase boundary movement and that the current transient technique has been proposed as a useful method to evaluate the degree of β-hydride phase formation, time to decomposition of the β-hydride phase into α-phase, and hydrogen content in the electrode.

The present work considers the evaluation of performance of $LaNi_{4.7}Al_{0.3}$ and $LaNi_5$ porous electrodes used as anodes in Ni/MH secondary batteries. For this purpose, current decay transients were measured on the $LaNi_{4.7}Al_{0.3}$ and $LaNi_5$ porous electrodes in aqueous 6 M KOH solution and analyzed. The performance of $LaNi_{4.7}Al_{0.3}$ and $LaNi_5$ electrodes were evaluated with reference to the discharge capacity and β- to α-phase transition time.

2. Experimental

$LaNi_{4.7}Al_{0.3}$ and $LaNi_5$ (Aldrich Chem. Co., purity 99%) were first pulverized by grinding into fine powders having an average particle size of less than about 45 μm (325 mesh). These powders were mixed with 5 wt.% Ni powder and NMP (*N*-methyl pyrrolidone) solution containing the polymeric binder PVDF (poly-vinylidene fluoride) to make a slurry with a syrupy viscosity. The amount of the binder solution was adjusted to 5 wt.% PVDF for the $LaNi_{4.7}Al_{0.3}$ and $LaNi_5$ electrodes in the final specimen. The electrode specimens were prepared by spreading the slurry on Ni foam as a current collector, followed by drying under vacuum at 120°C for 2 h and then pressing at 17.2 MPa.

* Corresponding author.

PII S0378-7753(96)02647-X

Prior to use, the fresh $LaNi_{4.7}Al_{0.3}$ and $LaNi_5$ porous electrodes were activated through ten charge–discharge cycles by a charge–discharge controller (Toyo System Co., Ltd. HRC 6064A). The charging step was conducted at 100 mA g^{-1} for 3 h and discharging at 50 mA g^{-1} to −0.6 V (versus Hg/HgO) after a rest time of 600 s. The activated $LaNi_{4.7}Al_{0.3}$ and $LaNi_5$ electrode specimens were used as working electrodes. The electrolyte used was aqueous 6 M KOH solution. A platinum net and a mercury oxide electrode (6 M KOH/HgO/Hg) were used as a counter electrode and a reference electrode, respectively.

Current decay transients (chronoamperograms) on $LaNi_{4.7}Al_{0.3}$ and $LaNi_5$ porous electrodes were measured as functions of charging time and current densities from 50 to 250 mA g^{-1} by using a potentiostat (EG&G PAR, model 273) interfaced with an IBM-compatible computer. After hydrogen was galvanostatically charged in aqueous 6 M KOH solution, the electrode potential was suddenly moved to −0.6 V (versus Hg/HgO) in the same solution. From this moment, the resulting anodic current was recorded with time (current decay transient). The discharged hydrogen capacity was calculated by integrating the current decay transients with respect to time.

3. Results and discussion

Fig. 1 presents a typical current decay transient in logarithmic scale, log i versus log t, during the hydrogen discharging obtained from the $LaNi_{4.7}Al_{0.3}$ porous electrode previously hydrogen-charged at a current density of 100 mA g^{-1} for 1800 s in aqueous 6 M KOH solution. The three-staged current decay transient is composed of a current plateau, then a sudden fall of current with time, followed by a concave downward curve. Also, the current decay obtained from the $LaNi_5$ porous electrode galvanostatically charged has just the same shape. The transition time t_T value was measured as the time at which the tangent line of the first stage curve intersects that of the second stage curve.

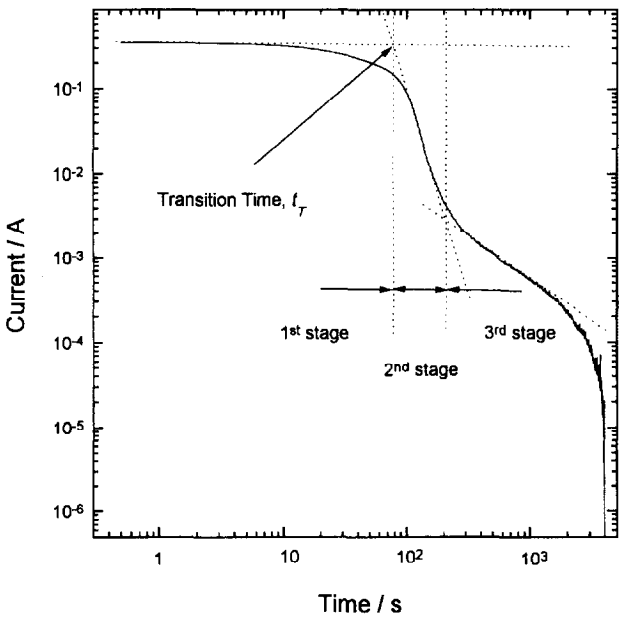

Fig. 1. Typical current decay transient in logarithmic scale, log i vs. log t, after moving the electrode potential to −0.6 V (vs. Hg/HgO) on an $LaNi_{4.7}Al_{0.3}$ porous electrode galvanostatically pre-charged at a current density of 100 mA g^{-1} for 1800 s in aqueous 6 M KOH solution.

From previous work [11–13] on current decay transient analysis, the appearance of three-staged current transients is caused by hydrogen transport through the $LaNi_{4.7}Al_{0.3}$ and $LaNi_5$ electrodes in the coexistence of two hydride phases α-phase (α-$LaNi_{4.7}Al_{0.3}H_x$; α-$LaNi_5H_x$) and β-phase (β-$LaNi_{4.7}Al_{0.3}H_y$; β-$LaNi_5H_y$) ($x<y$). Upon hydrogen discharging from both electrodes in the coexistence of α- and β-phase, the hydrogen transport seems to involve the following three steps:

(i) hydrogen transport through the electrode in the β-phase layer that is completely embedded in α-phase matrix runs by 'up-hill diffusion' of hydrogen, accompanied by interface-controlled phase boundary movement;

(ii) hydrogen transport goes to decomposition of the α-phase by simple diffusion;

(iii) the hydrogen transport is governed by decomposition of the remaining sporadic β-phase patches into α-phase.

Fig. 2(a) and (b) shows the current decay transients in logarithmic scale, log i versus log t, during the hydrogen discharging obtained from the $LaNi_{4.7}Al_{0.3}$ pre-charged porous electrode at 50 mA g^{-1} and $LaNi_5$ pre-charged porous electrode at 200 mA g^{-1}, respectively, in aqueous 6 M KOH solution at the various charging times indicated in Fig. 2. As the hydrogen charging time was prolonged, duration of the current plateau in the initial stage was significantly extended.

The three-staged current decay transients obtained from the $LaNi_{4.7}Al_{0.3}$ porous electrode had almost the same appearance and duration of the first stage current plateau (amounting to about 2.5×10^2 s) for hydrogen charging times above 1.8×10^4 s. This means that for the pre-charged electrode specimen, nearly the same time is required for decomposition of the completely embedded β-phase layer into α-phase and β-phase patches.

Thus, applying the charging current density of 50 mA g^{-1} above 1.8×10^4 s to the electrode specimen, the β-phase layer previously formed during the charging probably showed almost the same thickness value.

The three-staged current transients obtained from the $LaNi_5$ porous electrode had a similar shape to those from the $LaNi_{4.7}Al_{0.3}$ porous electrode. The duration of the first stage current plateau was about 1.3×10^2 s for hydrogen charging times above 2.7×10^3 s. This duration was much smaller than that from the $LaNi_{4.7}Al_{0.3}$ electrode, indicating that the thickness of the β-$LaNi_5H_y$ layer was much smaller than that of the β-$LaNi_{4.7}Al_{0.3}H_y$ layer.

The discharge capacities obtained from the $LaNi_{4.7}Al_{0.3}$ and $LaNi_5$ porous electrodes are plotted against charge capacity at various charging current densities in Fig. 3(a) and (b), respectively. The discharge capacity of the $LaNi_{4.7}Al_{0.3}$ elec-

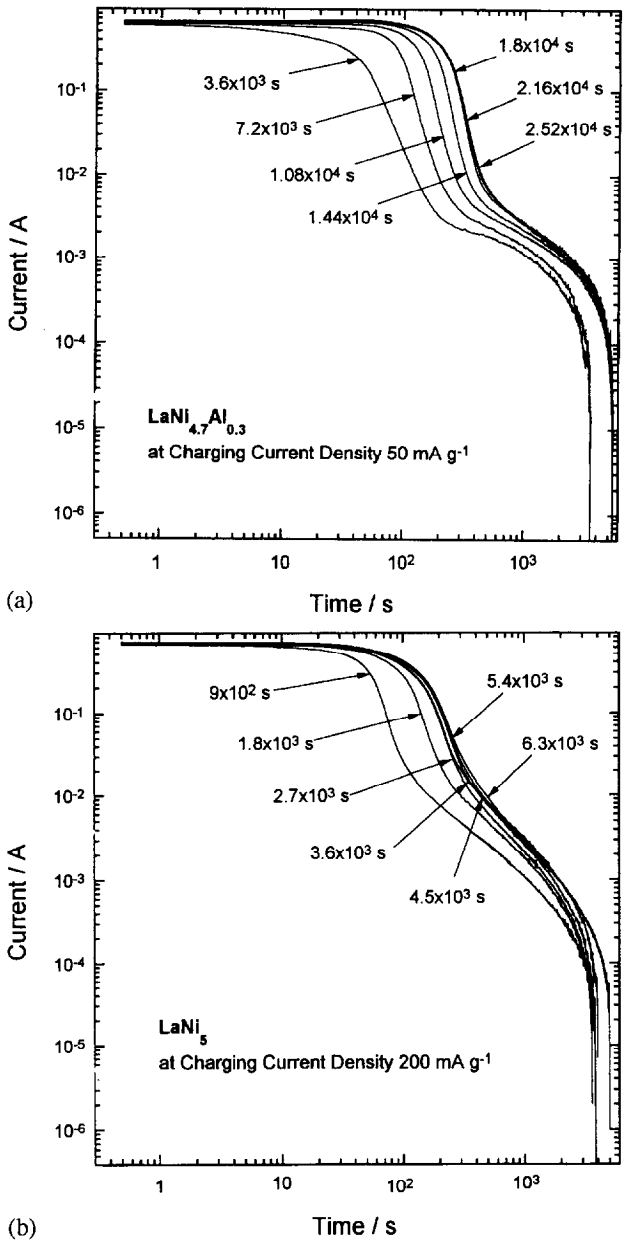

Fig. 2. Current decay transients in logarithmic scale, log i vs. log t, after moving the electrode potential to −0.6 V (vs. Hg/HgO) on (a) $LaNi_{4.7}Al_{0.3}$ porous electrode galvanostatically pre-charged at a current density of 50 mA g^{-1} and (b) $LaNi_5$ porous electrode at a current density of 200 mA g^{-1} in aqueous 6 M KOH solution for various times.

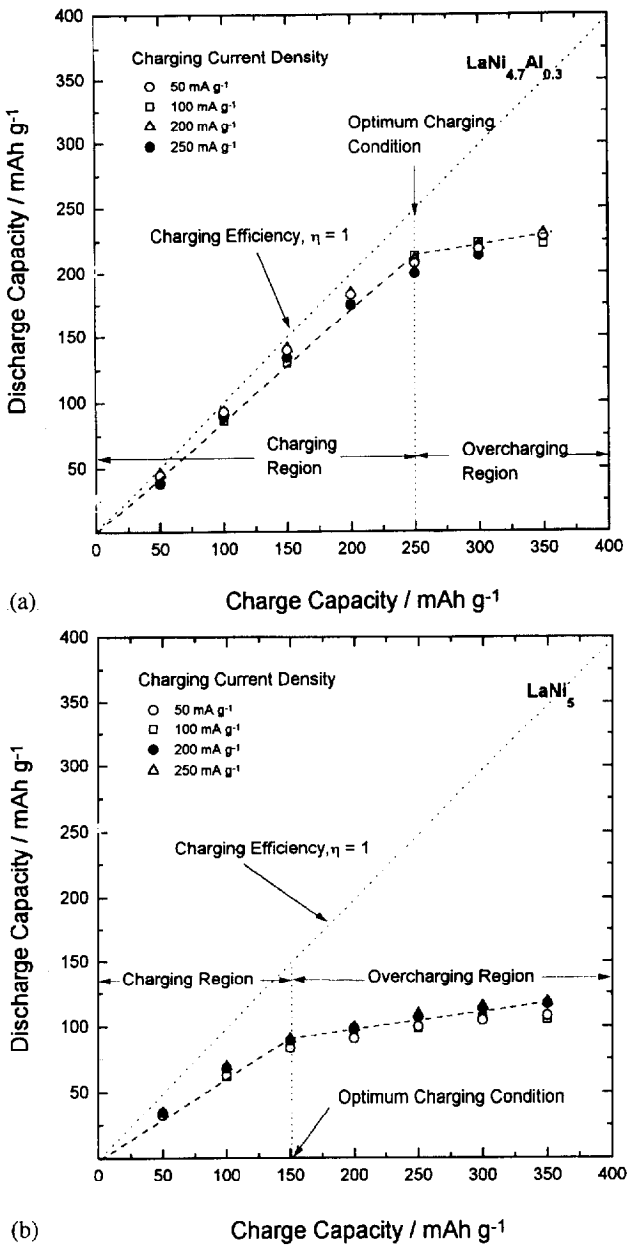

Fig. 3. Plots of discharge capacity against charge capacity of (a) $LaNi_{4.7}Al_{0.3}$ and (b) $LaNi_5$ porous electrodes in aqueous 6 M KOH solution at charging current densities of: ○, 50; □, 100; △, 200; ●, 250 mA g^{-1}.

trode linearly increased with increasing charge capacity up to 250 mAh g^{-1} and then slightly increased, regardless of hydrogen charging current density. The discharge versus charge capacity curve can be divided into two regions characterized by a sudden change in the slope of the curve. Those curves obtained from the $LaNi_5$ electrode showed almost the same shape. However, the maximum discharge capacity was much smaller than that from the $LaNi_{4.7}Al_{0.3}$ electrode. The $LaNi_{4.7}Al_{0.3}$ and $LaNi_5$ electrodes showed maximum discharge capacities of about 230 and 120 mAh g^{-1}, respectively.

Now we could define the charging efficiency η as the ratio of discharge capacity to charge capacity. If all the hydrogen atoms charged into the electrode are completely discharged, then the charging efficiency should be unity in value (dotted straight line with 45° slope in Fig. 3(a) and (b)). The first region line deviates weakly from the ideal charging efficiency of unity, while the second region line shows a strong deviation. In fact, the measured charge capacity is not only due to the absorbed hydrogen, but also to the evolved hydrogen, since the hydrogen charging into the MH electrodes in general involves hydrogen evolution and absorption reactions [14]. The hydrogen discharging is in part impeded by the surface oxide layer [5] and in part hindered by hydrogen trapping in the electrode [15]. The strong deviation $(1-\eta)$ comprises

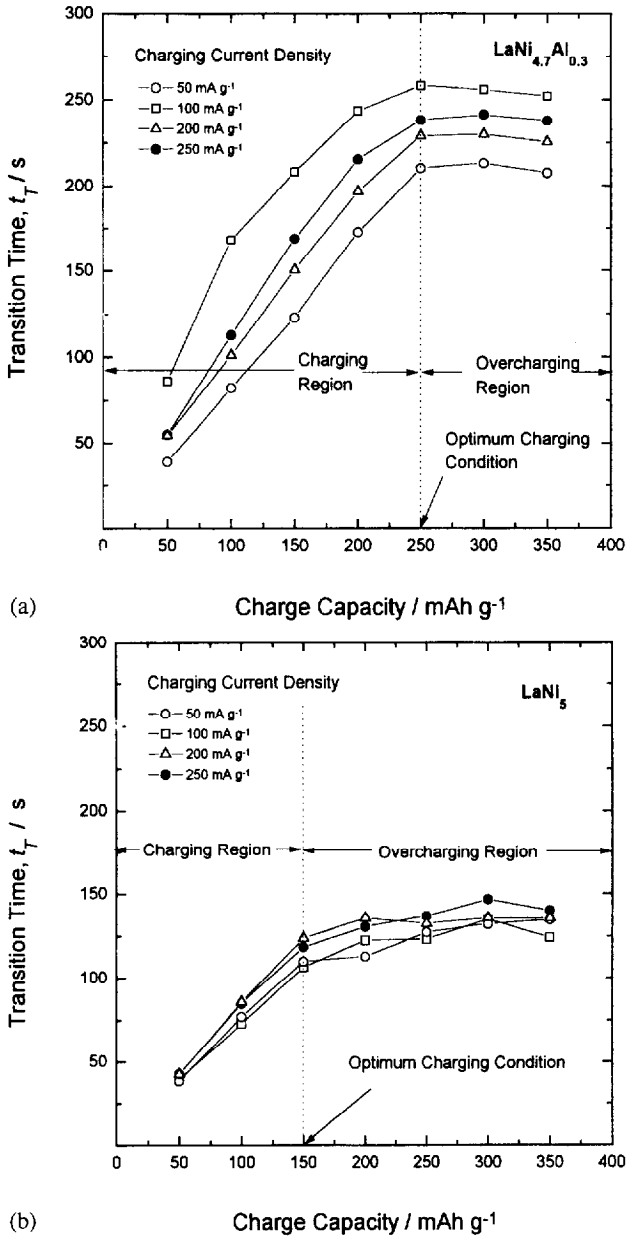

Fig. 4. Plots of transition time t_T against charge capacity of (a) $LaNi_{4.7}Al_{0.3}$ and (b) $LaNi_5$ porous electrodes in aqueous 6 M KOH solution at charging current densities of: ○, 50; □, 100; △, 200; ●, 250 mA g^{-1}.

the contribution of hydrogen evolution, discharging retardation by the oxide layer and hydrogen trapping. Therefore, we can regard the second region as the overcharging area and hence propose the optimum charging conditions of 250 mAh g^{-1} for the $LaNi_{4.7}Al_{0.3}$ electrode and 150 mAh g^{-1} for the $LaNi_5$ electrode.

In order to consider the optimum charging conditions in another way, the transition time t_T is plotted against charge capacity for the $LaNi_{4.7}Al_{0.3}$ and $LaNi_5$ porous electrodes at various charging current densities in Fig. 4(a) and (b), respectively. The t_T values were rapidly raised with increasing charge capacity up to 250 mAh g^{-1} for the $LaNi_{4.7}Al_{0.3}$ electrode and up to 150 mAh g^{-1} for the $LaNi_5$ electrode, and then attained the saturated values at all charging current densities for both electrodes. The t_T versus charge capacity curves can be classified into two regions characterized by a sudden slope change. The value of the saturation t_T in the second region depended on charging current density. The maximum saturation transition times t_T were found to be 250 s for the $LaNi_{4.7}Al_{0.3}$ electrode and 140 s for the $LaNi_5$ electrode.

From previous work [11–13], the transition time t_T represents the time to decomposition of the completely embedded β-phase layer in the α-phase into α-phase and β-phase patches by α/β phase boundary movement. This means that t_T is identical to the time necessary for the α/β phase boundary to reach the electrode surface from inside the electrode. Provided that the electrode is composed of uniformly distributed MH particles in size and the velocity of the α/β phase boundary is constant irrespective of charging current density, the reduction in saturation t_T with respect to charging current density means a decrease in particle size which is probably caused by the pulverization of $LaNi_{4.7}Al_{0.3}$ and $LaNi_5$ particles during the hydrogen charging.

From the slight increase of discharge capacity (Fig. 3(a) and (b)) and saturation of transition time t_T (Fig. 4(a) and (b)) with the charge capacity in the second region, it is inferred that the β-phase layer grows to a certain thickness in the first region, surrounding the α-phase matrix and it is transformed into a thin β'-phase layer just beneath the electrode surface in the second region. The phase transition from β to β' in general means a fall in equilibrium hydrogen absorption potential, i.e. a rise in equilibrium hydrogen absorption pressure [6]. The hydrogen atoms contained in the β'-phase are easily self-discharged since the equilibrium hydrogen pressure of the β'-phase is much higher than 1 bar. Thus, the hydrogen in the β'-phase hardly contributes to the discharge capacity. Therefore, we can consider the second region as the overcharging field and hence propose the optimum charging conditions of 250 mAh g^{-1} for the $LaNi_{4.7}Al_{0.3}$ electrode and 150 mAh g^{-1} for the $LaNi_5$ electrode. The optimum charging conditions obtained from the t_T versus charge capacity curves (Fig. 4) are in good agreement with those obtained from the discharge versus charge capacity curves (Fig. 3).

The velocity of α/β phase boundary movement can be simply calculated by dividing the effective radius of the MH particle by the maximum saturation t_T, assuming that the uniformly distributed MH particles are scarcely pulverized during the activation of the electrode, maintain the as-prepared state and have the same size as the β-phase layer (surrounding the α-phase matrix) formed during the charging in thickness. In the present work, the thickness of the β-phase layer with planar symmetry is equivalent to the effective radius $r/3$ for the radius r of the as-prepared $LaNi_{4.7}Al_{0.3}$ particle with spherical symmery. The velocity of phase boundary movement in the $LaNi_{4.7}Al_{0.3}$ electrode was determined to be about 3×10^{-6} cm s^{-1} from the values of particle size 45 μm (the effective radius 7.5 μm) and maximum saturation t_T 250 s.

4. Conclusions

The present work is aimed at evaluating the performance of $LaNi_{4.7}Al_{0.3}$ and $LaNi_5$ porous electrodes in the coexistence of the hydrogen-poor α-phase and hydrogen-rich β-phase by current decay transients analysis. The optimum charging condition was found more readily by using the potentiostatic decay transient technique, as compared to the galvanostatic charge–discharge technique commonly used.

From the current decay transients analysis, the maximum values of discharge capacity were calculated to be about 230 mAh g^{-1} for the $LaNi_{4.7}Al_{0.3}$ electrode and 120 mAh g^{-1} for the $LaNi_5$ electrode. The transition time t_T represents the time to decomposition of the β-phase layer into α-phase and β-phase patches. The maximum values of t_T were determined to be about 250 s for the $LaNi_{4.7}Al_{0.3}$ electrode and 140 s for the $LaNi_5$ electrode.

The optimum charging condition can be regarded as the charge capacity up to the saturation t_T value. From the measured discharge capacity and saturation transition time t_T, the optimum charging condition with respect to the charge capacity was found to be about 250 mAh g^{-1} for the $LaNi_{4.7}Al_{0.3}$ electrode and 150 mAh g^{-1} for the $LaNi_5$ electrode.

The velocity of α/β phase boundary movement in the $LaNi_{4.7}Al_{0.3}$ electrode was estimated to be 3×10^{-6} cm s^{-1} from the effective radius 7.5 μm (particle size 45 μm) and saturation time to β- to α-phase transition 250 s.

Acknowledgements

The authors are grateful to the Korea Science and Engineering Foundation 1996/99 (contract No. 96-0300-17-0-3) for the financial support of this work.

References

[1] F. Bittner and C.C. Badcock, *J. Electrochem. Soc., 130* (1983) 193C.
[2] J.J.G. Willems and K.H.J. Buschow, *J. Less-Common Met., 129* (1987) 14.
[3] M. Kanda, M. Yamamoto, K. Kanno, Y. Satoh, H. Hayashida and M. Suzuki, *J. Less-Common Met., 172–174* (1991) 1227.
[4] T. Sakai, H. Miyamura, N. Kuriyama, H. Ishikawa and I. Uehara, *Z. Phys. Chem., 183* (1994) 333.
[5] A.H. Boonstra, G.J. Lippits and T.N.M. Bernards, *J. Less-Common Met., 155* (1989) 119.
[6] C. Iwakura, Y. Kajiya, H. Yoneyama, T. Sakai, K. Oguro and H. Ishikawa, *J. Electrochem. Soc., 136* (1989) 1351.
[7] T. Sakai, A. Takagi, K. Kinoshita, N. Kuriyama, H. Miyamura and H. Ishikawa, *J. Less-Common Met., 172–174* (1991) 1194.
[8] D. Linden, in D. Linden (ed.), *Handbook of Batteries*, McGraw-Hill, New York, 2nd edn., 1994, p. 33.1.
[9] M. Mueller, J.P. Blackledge and G.G. Libowitz, *Metal Hydrides*, Academic Press, New York, 1968, p. 633.
[10] E. Wicke, H. Brodowsky and H. Züchner, in G. Alefeld and J. Völkl (eds.), *Hydrogen in Metal II*, Springer, Berlin, 1978, p. 73.
[11] T.-H. Yang, S.-I. Pyun and Y.-G. Yoon, *Electrochim. Acta*, (1997) in press.
[12] T.-H. Yang and S.-I. Pyun, *Electrochim. Acta*, (1996) submitted for publication.
[13] Y.-G. Yoon and S.-I. Pyun, *Electrochim. Acta*, (1996) accepted for publication.
[14] T.-H. Yang and S.-I. Pyun, *J. Power Sources*, (1996) in press.
[15] Ch.A. Wert, in G. Alefeld and J. Völkl (eds.), *Hydrogen in Metal II*, Springer, Berlin, 1978, p. 305.